Environmental Science and Pollution Research (2018) 25:12515–12527
https://doi.org/10.1007/s11356-018-1429-0

RESEARCH ARTICLE

Using a multi-method approach based on soil radon deficit, resistivity, and induced polarization measurements to monitor non-aqueous phase liquid contamination in two study areas in Italy and India

Mauro Castelluccio[1] · Sudha Agrahari[2] · Gabriele De Simone[1] · Francesca Pompilj[1] · Carlo Lucchetti[1] · Debashish Sengupta[2] · Gianfranco Galli[3] · Pierluigi Friello[4] · Pierpaolo Curatolo[5] · Riccardo Giorgi[5] · Paola Tuccimei[1]

Received: 26 May 2017 / Accepted: 29 January 2018 / Published online: 20 February 2018

Abstract

Geochemical and geophysical surveys employing radon deficit, resistivity, and induced polarization (IP) measurements were undertaken on soil contaminated with non-aqueous phase liquids (NAPLs) in two different sites in India and in Italy. Radon deficit, validated through the comparison with average soil radon in reference unpolluted areas, shows the extension of contamination in the upper part of the unsaturated aquifers. In site 1 (Italy), the spill is not recent. A residual film of kerosene covers soil grains, inhibiting their chargeability and reducing electrical resistivity difference with background unpolluted areas. No correlation between the two parameters is observed. Soil volatile organic compounds (VOCs) concentration is not linked with radon deficit, supporting the old age of the spillage. NAPL pollution in sites 2a and 2b (India) is more recent and probably still active, as demonstrated by higher values of electrical resistivity. A good correlation with IP values suggests that NAPL is still distributed as droplets or as a continuous phase in the pores, strengthening the scenario of a fresh spill or leakage. Residual fraction of gasoline in the pore space of sites 2a and 2b is respectively 1.5 and 11.8 kg per cubic meter of terrain. This estimation is referred to the shallower portion of the unsaturated aquifer. Electrical resistivity is still very high indicating that the gasoline has not been strongly degraded yet. Temperature and soil water content influence differently radon deficit in the three areas, reducing soil radon concentration and partly masking the deficit in sites 2a and 2b.

Keywords NAPL contamination · Soil radon · Soil electrical resistivity · Soil induced polarization · Environmental monitoring · Italy · India

Introduction

Detection and monitoring of organic contaminants, e.g., non-aqueous phase liquids (NAPLs), within the subsurface using non-invasive geochemical and geophysical methods are crucial due to its direct impact primarily on groundwater resources. The presence of NAPLs in the subsurface is mainly due to spills or leakages from storage tanks and pipelines. Groundwater solubility of these pollutants is low but their toxicity may decrease water quality. NAPLs may persist in the subsurface for long periods, sometimes for centuries, thereby becoming long-term sources of groundwater contamination (Zhang et al. 1998).

After moving downward through the vadose zone, some light NAPLs (LNAPLs) float and move on top of the water table, while denser NAPLs (DNAPLs) migrate downward and penetrate into the saturated zone. Within the vadose zone,

Responsible editor: Georg Steinhauser

Electronic supplementary material The online version of this article (https://doi.org/10.1007/s11356-018-1429-0) contains supplementary material, which is available to authorized users.

✉ Paola Tuccimei
paola.tuccimei@uniroma3.it

[1] Dipartimento di Scienze, Università degli Studi Roma Tre, Largo San Leonardo Murialdo 1, 00146 Rome, Italy

[2] Department of Geology and Geophysics, Indian Institute of Technology, Kharagpur, West Bengal 721302, India

[3] Istituto Nazionale di Geofisica e Vulcanologia, Sezione Roma 1, Via di Vigna Murata 605, 00143 Rome, Italy

[4] Polo Geologico s.r.l., Lungotevere degli Inventori 114 B, 00146 Rome, Italy

[5] Golder Associates, Via Sante Bargellini 4, 00157 Rome, Italy

NAPLs exist as pool or individual blobs (Mackay and Cherry 1989) indicating the occurrence of the contaminant plume. In the frame of the current work, a multi-method approach, based on soil radon deficit, resistivity, and induced polarization (IP) measurements, was employed to study the spatial distribution of residual contaminants in the aquifer and infer information on groundwater contamination. Radon deficit was focused on the vadose zone of the aquifer, while resistivity and IP surveys investigated the subsoil giving information on both the unsaturated and saturated zones. This has important ramifications in heavily stressed groundwater regions like the Indian subcontinent, where groundwater-fed irrigated areas have increased from 30% in 1960 to ~ 50% in 1995 (Scanlon et al. 2010) and has been further increasing in recent years.

Soil radon is used as tracer of NAPL contamination because it is extremely soluble in these substances and produces a concentration-deficit compared to nearby unpolluted areas. The mapping of this process, known as "radon-deficit technique" (Semprini et al. 2000) allows to identify the contamination affecting the vadose zone. An excellent review on that with an exhaustive list of related references has been recently published (Schubert 2015). Based on the Eq. (1) reported in Schubert (2015), which correlates soil radon activity concentration (C_∞) with NAPL fraction in the pore space, De Simone et al. (2017) developed a new calculation, Eq. (2), to quantify the residual fraction of NAPL ($NAPL_{Pi}$) in the subsoil (unsaturated part of the aquifer). Both equations are listed as follows:

$$C_\infty = \varepsilon A_{Ra}\rho_d/n\left(1-S_F + K_{W/SG}S_F(1-X_{NAPL}) + K_{NAPL/SG}X_{NAPL}S_F\right) \quad (1)$$

where

C_∞	Radon concentration in the soil pore space (Bq/m^3)
ε	Emanation coefficient
A_{Ra}	^{226}Ra activity concentration of the mineral matrix (Bq/kg)
ρ_d	Bulk density of the mineral matrix (kg/m^3)
n	Porosity of the mineral matrix
S_F	Total fluid saturation of the pore space
X_{NAPL}	NAPL fraction of S_F
$K_{W/SG}$	Radon partition coefficient between water and soil gas, quantified by Weigel (1978)
$K_{NAPL/SG}$	Radon partition coefficient between NAPL and soil gas

$$NAPL_{Pi} = \frac{-J \pm \sqrt{J^2-4CH}}{2H} \quad (2)$$

where

J, C, H: site-specific polynomials whose explanation is provided in the Appendix.

Resistivity and induced polarization methods are applied to detect NAPLs in soils, with a variety of results related to NAPL distribution in soil pores. Recently, Johansson et al. (2015) reported on possible conceptual models showing how residual NAPL configurations in porous media affect measured IP responses. The four models assume that NAPL is distributed as follows: (a) isolated droplets in the pores or (b) trapped in the pore throats and (c) as a continuous phase through several pores or (d) as coatings around soil grains. These configurations influence IP spectral parameters providing hints for residual free-phase NAPL distribution and for the ongoing natural or in-situ stimulated biodegradation. The IP method extends the resistivity method by making an additional measurement of the ability of the ground to store electrical charges. It was initially developed for mineral exploration, but it is now extensively applied to environmental and engineering geophysics. IP measures both the conductive and capacitive properties of the sub-surface (Slater and Lesmes 2002). It has also been hypothesized that hydrocarbon spills may lead to changes in the electrical properties of the aquifers over time, from resistive to conductive due to bio-degradation (Sauck et al. 1998; Che-Alota et al. 2009).

The aim of this work is the joint application of these two approaches to assess soil contamination by NAPLs in two study areas located in Italy (site 1) and India (sites 2a and 2b). The site characteristics are very different not only from the geological and climatological point of view, but also in terms of spills age and kind of released substance. The results of soil radon surveys in site 1 have been recently published (De Simone et al. 2017), whereas resistivity and induced polarization measurements are original. Gasoline spills in India are presented here for the first time.

The joint discussion of the main results obtained for these two locations allows us to emphasize the potential of this multi-method approach in the study of soil NAPL contamination in case of old and also recent spills, with focus to different contamination depths.

Study areas

The two study areas are located in Italy (site 1) and India (sites 2a and 2b). The site characteristics are very different not only from the geological and climatological point of view, but also in terms of spills age and type of released substance.

Site 1 (Italy)

Site 1 is located in a coastal area, within a river delta (Latium Region, Italy), but its location and coordinates are omitted for confidentiality agreement. The bedrock from top to bottom mainly consists of about 0.5 m of backfills, 2.5 m of medium grained sands and at least 10 m of medium-fine-grained sands. The water table fluctuates in the range 0.5–2.5 m below the ground during the year (Tuccimei et al. 2014), 2.5 m during the 2016 winter survey.

The area is located at the margin of a large volcanic-geothermal province and is characterized by extensive CO_2 release both from localized manifestations and diffuse degassing (Rogie et al. 2000; Chiodini and Valenza 2007; Carapezza et al. 2012). The CO_2 is associated with deep geothermal reservoirs, hosted in the Meso-Cenozoic carbonate rock successions that outcrop in the Apennines. Allochthonous argillitic flysch and post-orogeny Neogene marine clayey succession seal the reservoir atop (Giordano et al. 2016 and references therein).

The climate is Mediterranean with dry summers and mild, moist winters. The kerosene spill occurred more than 10 years ago. An overall description of the area is provided in De Simone et al. (2017).

Site 2 (India)

Site 2 is located in Kharagpur area (West Bengal, India; Fig. 1). Two different spill sites, site 2a and 2b, located in close proximity, were investigated using a multi-method approach based on soil radon deficit, resistivity, and induced polarization measurements. The study area lies between latitudes 22° 12′ 0″ to 22° 23′ 0″ N and longitudes 87° 12′ 30″ to 87° 18′ 0″ E (Fig. 1). The rainy season in the region prevails from the months of July to September with an average rainfall of 307 mm per month. The average temperature during monsoon is ~ 28.9 °C. Summer average temperature is ~ 31.5 °C, from April to June (Chatterjee et al. 2003–2004). Winter is brief but chilly, lasting from December to mid-February, with average temperatures of ~ 22 °C. Scarce information are available on the contamination event. Among few certain news, we know that gasoline leakage, probably slow and but continuous, has occurred from underground petrol tanks.

Soil in this area is primarily lateritic, with patches of alluvium (sand/silt dominant) in the north and with further smaller spots of alternating beds of sand/silt and clay in proximity of Kangsabati River (Fig. 1). Pedogenetic processes and groundwater flow are responsible for the high frequency of iron and aluminum nodules and concretions within the mottled

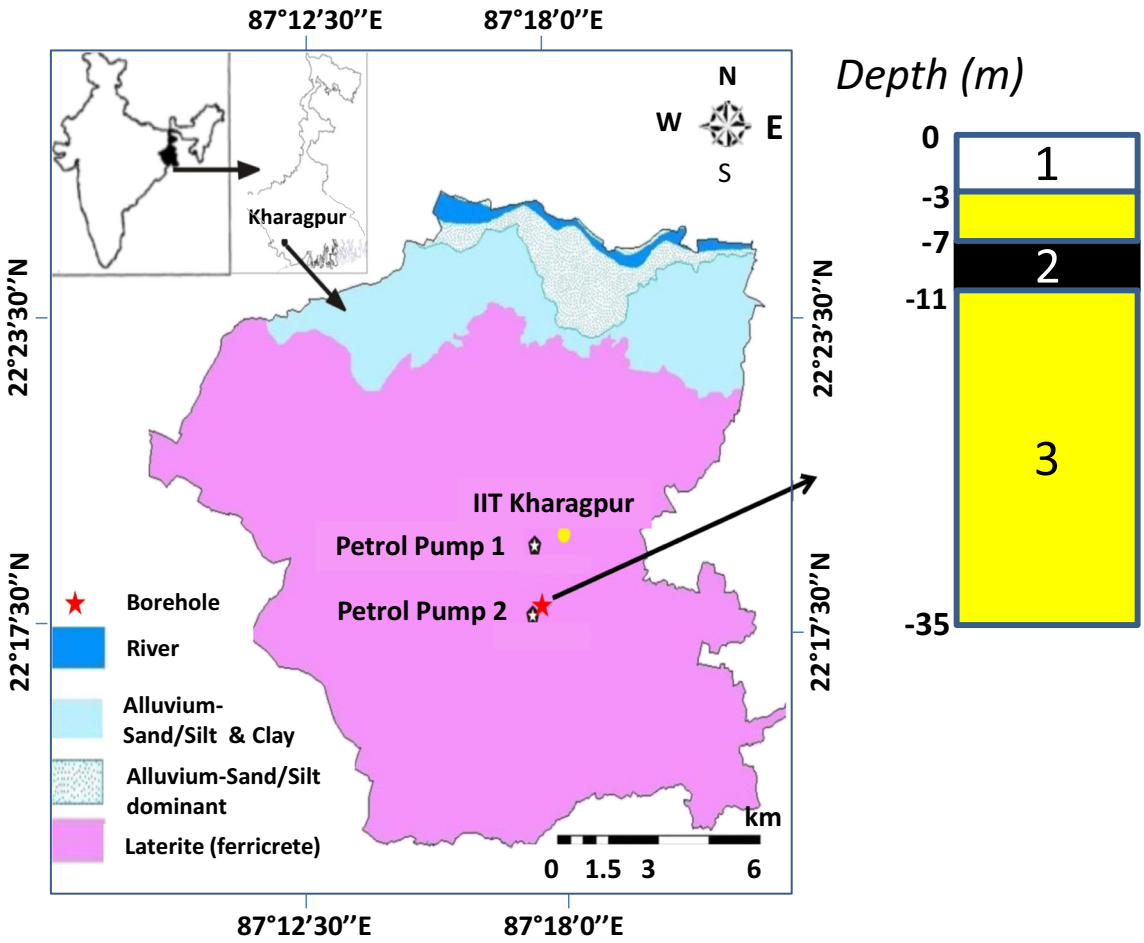

Fig. 1 Lithological map of Kharagpur area in West Bengal (India), with location of IIT campus, study sites 2a and 2b and borehole location. Information on the stratigraphy of the borehole are from Machiwal and Jha (2016). Labels 1, 2, and 3 stands for soil + murrum, coarse + medium sand, and coarse + medium to fine sands, respectively. Murrum is a local name for a reddish-brown colored hard-rock (lateritic bauxite). Surface geological map was provided by Irrigation and Waterways Department, Geological Division No. 1, State Water Investigation Directorate, Medinipur, West Bengal, India

horizon. Erosion removes soft topsoil up to the depth of the concretionary zone, which permanently hardens due to subaerial exposure forming the crust of indurated laterites (Chatterjee et al. 2003–04). Laterites becomes non-permeable at greater depths (> 1 m), enhancing the retention of water as well as of other liquids, in the subsoil. The general stratigraphy of the region, deduced by a borehole located in the study area (Fig. 1; see Machiwal and Jha 2016), consists of layers of coarse-medium grained sands alternated with levels of fine-grained sands.

Methods

A multi-method approach based on soil radon deficit, resistivity, and induced polarization measurements was applied in two study areas in Italy (site 1) and India (site 2) to evaluate the potential and limits of this integrated methodology.

Soil radon and intrinsic permeability determinations

Soil radon concentration was measured at 80-cm depth using a hollow probe manufactured by RADON v.o.s., connected to a RAD7 monitor (Durridge Company Inc.) through vinyl tubing. A small cylindrical cavity is created just below the probe head by the extrusion of a lost tip. The volume of the cavity (about 5.6 cm^3) is large enough to enable soil gas collection using the RAD7 built-in pump. Soil air is then dried, filtered, and delivered to RAD7 where radon (^{222}Rn and ^{220}Rn) decays into its daughter nuclides; they are collected onto the surface of the Si-detector and alpha-counted. The instrument separates polonium isotopes emitting alpha particles with different energies and provides the activity concentration of ^{222}Rn and ^{220}Rn, when correspondent equilibrium conditions are reached: about 15 min for ^{222}Rn (hereafter called radon) and few seconds for ^{220}Rn (also known as thoron). Soil radon activity is generally obtained by averaging data from the fourth and fifth 5-min cycles.

When the terrain is very humid, the water content in RAD7 may gradually increase, even if a desiccant is employed. In this case, radon activity concentration is progressively underestimated because of neutralization processes affecting radon daughters during electrostatic collection. Accordingly, proper corrections need to be applied to obtain reliable data (De Simone et al. 2016). On the other hand, carbon dioxide does not interfere with radon measurement, but a large flow of CO_2 may work as carrier for radon in the soil, favoring its transfer to the surface.

Soil gas permeability is obtained using PRM3 permeameter (Castelluccio et al. 2015). The instrument draws air from the same hollow probe used for radon measurement. The permeameter is equipped with a pump and a vacuum gauge that reads the negative pressure (ΔP), induced by soil gas extraction through the terrain. Intrinsic permeability is calculated according to a modified version of Darcy's equation where the air flow (Q) is replaced by a linear equation in the form: $Q = (m\ \Delta P + c)$, where m and c are respectively the slope and the intercept on Y-axis of the instrument calibration curve. For further details on it, the reader is referred to Castelluccio et al. (2015).

In winter 2016, soil radon concentration in site 1 was measured according to a special experimental configuration to investigate the role of kerosene vapors on soil radon distribution patterns (De Simone et al. 2016). Two RAD7 monitors were placed in-series and connected to the top of the hollow probe driven up to 80-cm depth; the first instrument was directly attached to the probe and received humid soil gas, which was counted and then conveyed to the second monitor through a drierite cylinder capturing moisture and eventually the NAPL volatile component with the radon dissolved into vapors. Readings from the two instruments were cross-calibrated through specifically designed laboratory experiments and compared.

In spring 2016, soil gas concentration was measured in sites 2a and 2b, according to the standard approach described above. Permeability was estimated using a flowmeter (0–1 L/min operating range) placed at RAD7 outlet, with lower air flow values qualitatively corresponding to lower intrinsic permeability conditions.

Maps of soil radon, VOCs, and NAPL residual fractions in the studied sites were obtained using the program Surfer by Golden Software, using the kriging method for geospatial data interpolation.

Resistivity and induced polarization measurements

Electrical resistivity techniques are based on the application of a constant direct current injected into the ground via two current electrodes and on the measurement of the resulting potential difference between two potential electrodes. Measuring equipment is based on multi-electrode and multi-core cable systems. During the measurement, each electrode alternatively acts as current or potential electrode and datasets are acquired along the whole profile. The location of current and potential electrodes is influenced by the array. Depending upon the survey geometry, apparent resistivity data are plotted in 2D cross section.

Induced polarization (IP) effect reflects the degree to which the subsurface is able to store electric charge, analogous to a leaky capacitor. It occurs when some electric current passes through a rock/soil. If the current is interrupted, a difference in potential, which decays with time, is observed. The rate of decay of this potential (induced polarization potential) depends on the rock lithology, its pore geometry, and water saturation.

Resistivity and induced polarization (IP) measurements in site 1 were carried out employing a Syscal PRO ten-channel electrical georesistivimeter (Iris Instrument) which allows to carry out 2D or 3D surveys combining several parallel sequences of electrodes located within two partially overlapping grids of measurements. Multi-channel acquisition of resistivity and IP data (up to 10 simultaneous readings) was obtained using two sets of 48 and 72 electrodes, connected in several lines to create 3D ground images. They were obtained by overlapping different planar images derived from the juxtaposition of linear contiguous profiles.

Two rectangular grids made by 15 × 5 and 4 × 12 linear spreads of steel electrodes were employed to create a 3D image of the resistivity and the chargeability of the subsoil. The first array was WNW-ESE oriented with a spacing between the electrodes of 7.5 m in the longest side (*x*-axis) and 2.5 m in the shortest side, with a total size of 35 × 30 m. The second array was NNE-SSW oriented with a spacing between the electrodes of 2.5 m in both sides with a total length of 27.5 m and a width of 7.5 m. It was chosen to overlap the two arrays of 7.5 × 7.5 m and to use a shorter interdistance in the second one because a more detailed image of that area was required, particularly in the NNE-SSW direction, which corresponds to the spill flow according to previous studies (De Simone et al. 2015, 2017). A pole-dipole array was employed, configured for a penetration of at least 3 m, which was approximately the groundwater table depth. Resistivity was measured during the injection of the direct current pulse, with a length of 250 ms, while chargeability was measured during voltage decay after the current was interrupted. IP corresponds to the integral of the decay curve during the defined time window of 500 ms. Tridimensional data analysis was performed by ERTLab software.

Resistivity and IP data at site 2a were acquired using a Terrameter LS (ABEM, Sweden) system. In the present study, Wenner-Schlumberger array configuration was adopted because it allows deeper penetration and has the ability to effectively resolve vertical and lateral subsurface features (Dahlin and Zhou 2004; Candansayar 2008). Twenty-three data levels were acquired along both ERT profiles. 2D inversion of the ERT data was performed using the "robust inversion" method which works well when the presence of internally homogeneous structures with sharp boundaries is expected (see stratigraphic column in Fig. 1). It was preferred to the "Gauss-Newton smoothness-constrained least-squares" method which tends to smooth excessively the boundaries in these cases. Processing and inversion of resistivity data were performed using RES2DINV code (Loke and Barker 1996; Loke 1997). Two resistivity and IP profiles, NW-SE and N-S oriented, were performed on the lateral side of the petrol pump. Both resistivity and IP datasets were collected along these lines. However, due to inaccessibility problems, one profile was 160 m long (profile 1; Fig. 3) and the other one 100 m long (profile 2; Fig. 3). The interelectrode spacing for profiles 1 and 2 was selected as 4 and 2.5 m, respectively. A square wave with a time period of 1 s was used for the measurements; full waveform data were recorded.

Results

Soil radon

Soil radon was measured and mapped in the two study areas in Italy and India in order to outline regions with lower activity concentrations to refer to NAPL in the subsoil and to estimate residual fractions of contaminants in the vadose zone.

Soil radon in site 1

The spill of kerosene occurred long time ago (about 10 years). After first investigations aimed at preparing site characterization and conceptual models reports, securing actions were implemented to temporarily isolate and remove the pollutant. In the frame of monitoring activities, soil gas (radon and carbon dioxide) and intrinsic permeability surveys were carried out in the study site and in nearby background areas in the years 2013, 2014, and 2016. They were repeated throughout the year to evaluate the effect of soil temperature and water content on seasonal changes of radon concentration and distribution in the soil pores. The climate is Mediterranean with dry summers and mild, moist winters. Winter campaigns gave better results compared to those carried out in spring, fall and summer because gas release at the soil-air interface is reduced in winter, due to the higher water content and lower temperature of soil, resulting in more marked differences at 80-cm depth between areas where radon is captured by kerosene (radon-deficit) and those characterized by natural activity concentrations (background). Radon winter maps, reported in De Simone et al. (2017), show a region of lower activity concentrations corresponding to the main spill and aligned along the groundwater flow induced by pneumatic pumps, as documented by Golder Associates. De Simone et al. (2017) also mapped the volatile organic compounds (VOCs; Fig. 3a) and the residual NAPL fractions in winter 2016 (Fig. 2b), calculated according to Eq. (2), demonstrating that at present radon deficit is not correlated (R^2 is equal to 0.084) and thus not dependent on NAPL vapors (VOCs) but is strictly correspondent and proportional to residual NAPL in the soil. This is compatible with the loss of the volatile fraction of kerosene in the upper part of the terrain, expected for a spill occurred more than 10 years ago. It follows that the residual component of kerosene produces the radon-deficit and can be used to calculate the average amount of NAPL still present in the site, which was estimated at 17 kg per cubic meter of terrain, in agreement with 23 kg of total hydrocarbon per cubic meter

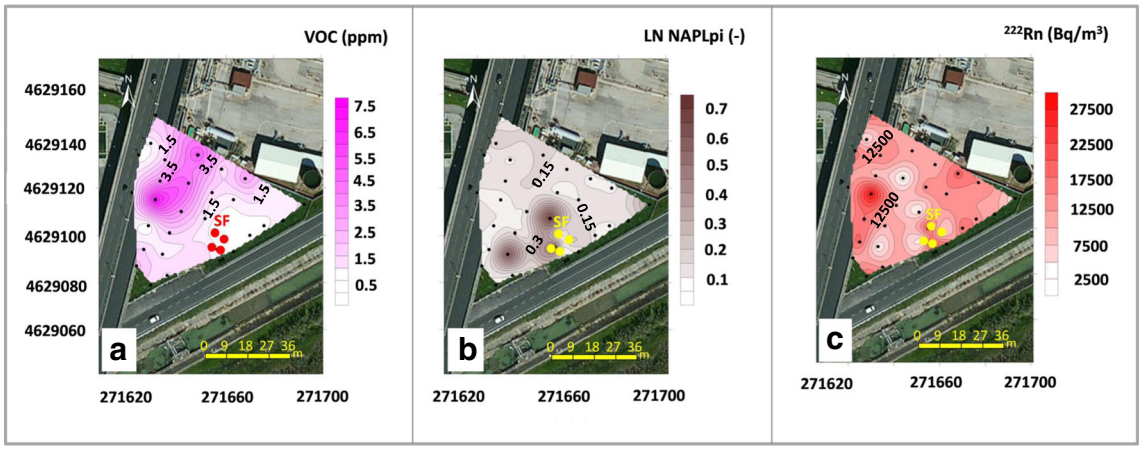

Fig. 2 Maps of soil VOCs (**a**), calculated fraction of residual kerosene (**b**) and soil radon activity concentration (**c**) obtained during winter 2016 (Fig. 8 in De Simone et al. 2017). The location of the reference station (SF) for soil temperature and water content and that of some nearby measuring points has been added as cross-reference with Fig. 4

directly measured in 2007, before the start of remediation actions (De Simone et al. 2017). See the Appendix for further details regarding the calculation of residual fraction of NAPL in the soil pores.

Soil radon in site 2

In spring 2016 (from late February to early April), soil gas concentration was measured in the area of Kharagpur (West Bengal, India), near two working petrol stations (sites 2a and 2b; Fig. 1), according to the standard approach described above, in order to investigate the possible presence of contaminant into the soil, outline its spatial distribution, and evaluate its amount in the vadose zone. Permeability was estimated using a flowmeter placed at RAD7 outlet, with lower air flows corresponding to lower intrinsic permeability conditions.

Measurements of soil radon concentration were performed around the petrol stations with a grid size of 5 m (Fig. 3). Soil

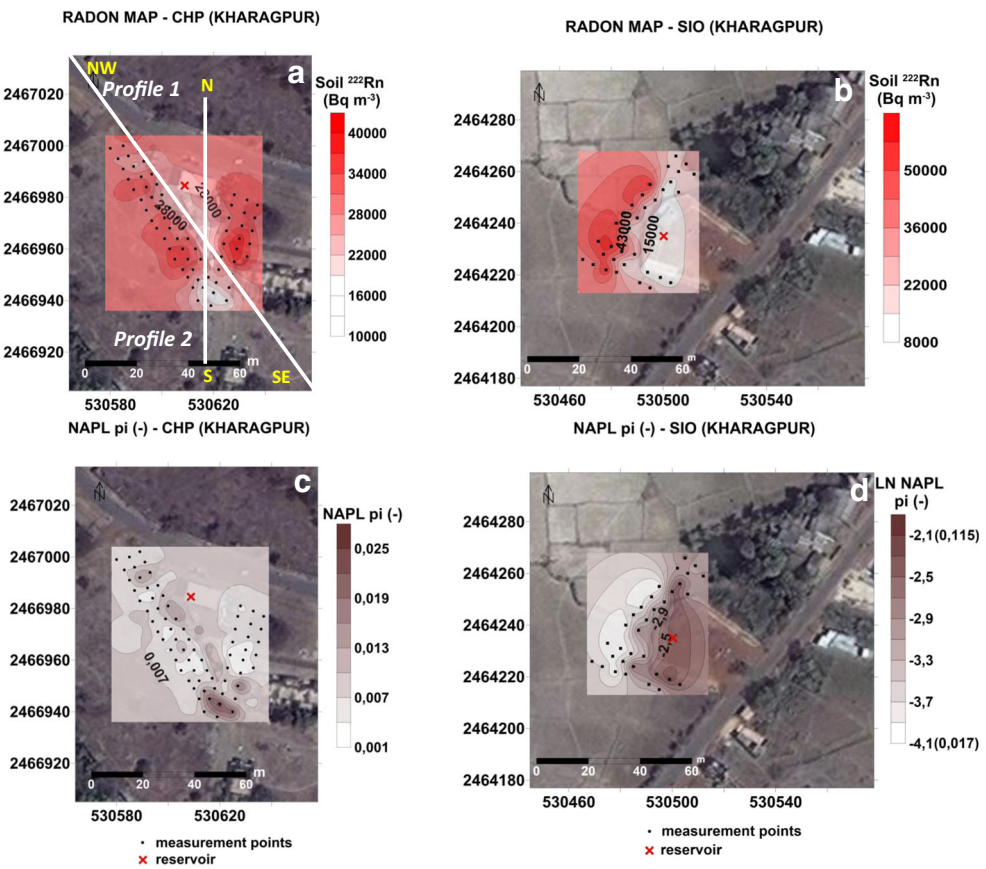

Fig. 3 Soil radon concentration maps of site 2a (**a**) and 2b (**b**) and calculated fraction of residual gasoline maps in site 2a (**c**) and 2b (**d**). A logarithmic function and scale was used in **d** to better interpolate data. Corresponding minimum and maximum residual gasoline fraction are reported in brackets for reference. Tracks of NW-SE trending profile 1 and N-S trending profile 2, where resistivity and induced polarization surveys were carried out, are indicated in **a**

radon data from adjacent sites with similar geological setting were used to define the radon level of correspondent uncontaminated areas (the so-called background sites) and calculate the radon-deficits (see Appendix). Background areas (100 m^2) were chosen at a distance of about 100 m from the reservoirs. Soil radon data were not corrected for high water content in RAD7 monitor because great care was kept to maintain this value low (De Simone et al. 2016).

Site 2a is very close to the IIT Kharagpur Campus. A total of 78 measurements were performed at a depth of 0.8 m, covering an area of about 3000 m^2. Average soil radon concentration is about 20 kBq m^{-3}, with minima of 13–15 kBq m^{-3} (Table S1). Correspondent background area is characterized by an average of about 33 kBq m^{-3} (minimum value of 28 kBq m^{-3}). Soil gas permeability is generally high.

Site 2b is located in Salua village at about 3 km south of IIT Kharagpur Campus. Intrinsic permeability is locally decreased by soil layers with different percentage of clay that slow down and partially prevent radon extraction. This induced us to collect radon at lower depth, up to 0.4 m from the ground. Forty-seven measurements over an area of about 2000 m^2 showed a gradual increase of soil radon concentration moving away from the tank (Table S2), where minimum values (8–10 kBq m^{-3}) were obtained. Background reference area is consistently characterized by an average soil radon concentration of 64 kBq m^{-3} (minimum value of 56 kBq m^{-3}).

Water content determinations carried out on three soil samples collected at 0.3-m depth at each site confirmed soil gas permeability estimation. Volumetric water contents were in the range of 4–8 and 23–25% for sites 2a and 2b, respectively. Low soil permeability in site 2b partly inhibited gas sampling leading to some anomalous values. Therefore, some radon values were excluded from mapping.

Evaluation of radon deficit and fraction of residual NAPL in the subsoil of sites 2a and 2b

Using the approach reported in De Simone et al. (2017), radon deficits and indicative fractions of residual gasoline ($NAPL_{Pi}$) in the vadose zone of sites 2a and 2b were tentatively estimated, although no analytical determinations of NAPL concentration in the soil matrix were available to validate the estimations. In this case, the approach is even reversed because we applied radon-deficit method to get preliminary information otherwise unavailable. See Appendix for a full description of the calculation. Parameters and polynomials used for that are reported in Tables S1 and S2. Table 1 lists the values of other calculation constraints. It is worth mentioning that the value of W_{Pi}, the fraction of water in the soil pores, has not been calculated using a reference station for soil humidity and temperature as in site 1 (De Simone et al. 2017), but employing the average of measured soil water contents, that is 6 and 24%, respectively for sites 2a and 2b. Fractions of residual NAPLs ($NAPL_{Pi}$) range from 0.0015 to 0.0240 in site 2a, with an average value of 0.0071 and from 0.0167 to 0.1156 in site 2b, with an average of 0.0497.

Finally, we can use the average fraction of residual NAPL in the pore space to evaluate the average volume of gasoline in a cubic meter of polluted terrain. Given a soil porosity of about 0.27 and 0.31, respectively for sites 2a and 2b, we have concluded that 270 and 310 L/m^3 are occupied by pores which retain an average of 1.9 and 15.4 L of NAPL per cubic meter. Since the density of gasoline is 0.755 kg/L, we can estimate about 1.5 and 11.8 kg of residual NAPLs in a cubic meter of terrain, respectively, in sites 2a and 2b.

Resistivity and induced polarization

Resistivity and IP surveys were carried out in study areas 1 and 2a, according to the methods described in a previous section.

Resistivity and induced polarization in site 1

In winter 2016, resistivity and induced polarization surveys were carried out in site 1. Results are shown in Fig. 4. A narrow region of higher resistivity (150–280 Ωm) is evident in the western side of the investigated area. It corresponds to the NNW-SSE trending soil radon-deficit segment described above and interpreted as due to the presence of residual NAPL

Table 1 Parameters used to calculate the fraction of NAPL in the pore space ($NAPL_{Pi}$) in sites 2a and 2b

Parameter	Symbol	Value[a]	Unit	Source
Specific weight of the solids	γ_s	2.65	g/cm^3	Conventionally assumed for silicate terrains
Moist specific weight	γ	2.05; 2.25	g/cm^3	Estimated on the basis of the average soil water content
Water specific weight	γ_w	1	g/cm^3	Assumed as for pure water
Gasoline specific weight	γ_{NAPL}	0.755	g/cm^3	Standard reference for marketed gasoline
Average soil 222Rn in the background	Rn_B	35,231; 57,836	Bq/m^3	This work
Radon partition coefficient between NAPL and soil gas at 23 °C	$K_{NAPL/SG}$	9.05	Fraction	Calculated from data in Schubert et al. (2007)

[a] When two values are quoted, the first is referred to site 2a and the second to site 2b

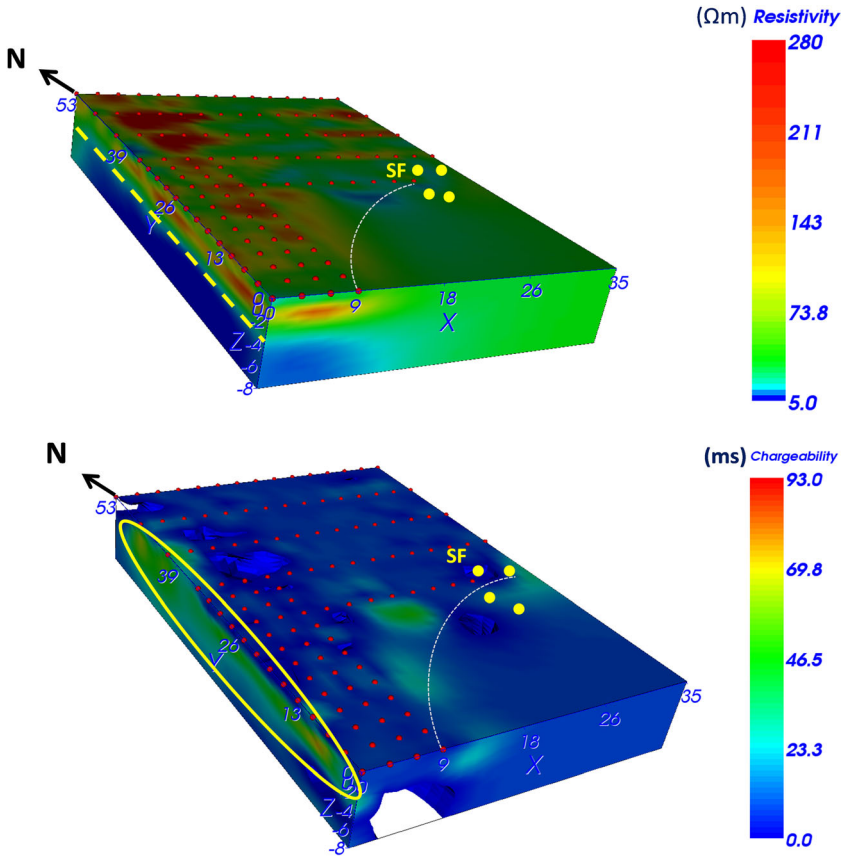

Fig. 4 3D maps of resistivity (**a**) and induced polarization (**b**) in site 1. The white arc indicates the limit of the grids and that of associated interpolated data. The location of the reference station (SF) for soil temperature and water content and that of some nearby measuring points has been added as cross-reference with Fig. 2. Units on the three axes are meters

(De Simone et al. 2017). Since NAPLs are actually electrical insulators, they cause rises in resistivity because their free-phase products may displace water in contaminated soil (Johansson et al. 2015). Surrounding soils, where residual NAPL is negligible, display much lower resistivity (10–80 Ωm), consistent with that measured for dry sands in the same area (Giordano et al. 2016). 3D electrical resistivity map also shows that residual NAPL is confined at depths lower than 2 m (especially in the upper meter) which is above the maximum level of local water-table fluctuation. Its top is located at about 2.5 m below the ground (Fig. 4a), as shown by the abrupt decrease of resistivity (below 5 Ωm) from that depth downward. The portion located from about 1 to 2 m depth shows intermediate resistivity (10–80 Ωm) because it is periodically washed by the rising water table, as documented by Golder Associates, reporting increased groundwater concentration of total hydrocarbon after periods of heavy rainfalls.

On the other hand, IP data are generally very low (< 20 ms) at surface, with no correlation with high resistivity or radon-deficit regions, but reach larger values (25–60 ms) where soil radon values are greater or along a NNW-SSE oriented area at depths higher than 2 m, which corresponds to the direction of the pumping-induced groundwater flow (Fig. 4b). We interpret low chargeability data at surface, in correspondence with radon-deficit areas, as due to pollutant residue in form of films, which coat soil particles, electrically isolating them, with no grain polarization (Johansson et al. 2015). Higher chargeability at surface may indicate no NAPL occurrence, while larger values at depth are likely due to the effect of contaminated soil leaching accomplished by pumping-securing actions implemented since the year 2007 to isolate the pollutant. Partial removal of residual kerosene films could be responsible for soil grains polarization.

Resistivity and induced polarization in site 2

Resistivity and IP surveys were carried out along two profiles at site 2a (Fig. 3). Two pseudo-sections are shown along each profile (Figs. 5 and 6), with the upper section corresponding to resistivity and the lower to IP models of the subsurface. The interpreted 2D ERT models along profiles 1 and 2 indicate that the depth of groundwater is presumably around 7–8 m below the surface. White dotted lines in the resistivity sections delimit high resistivity areas (400–800 Ωm), which could be interpreted as contaminated zones. Profile 2 intersects an area, about 10 m wide, with higher and constant resistivity (1000 Ωm) extending from 3 to 10 m depth, which could be the section of an underground storage tank (Fig. 6). From the bottom of that, a lower resistivity plume (700–900 Ωm) seems to extend at least up to 20 m depth.

Generally speaking, IP profiles show areas characterized by higher chargeability (up to 50 ms along profiles 1 and 2 in Figs.

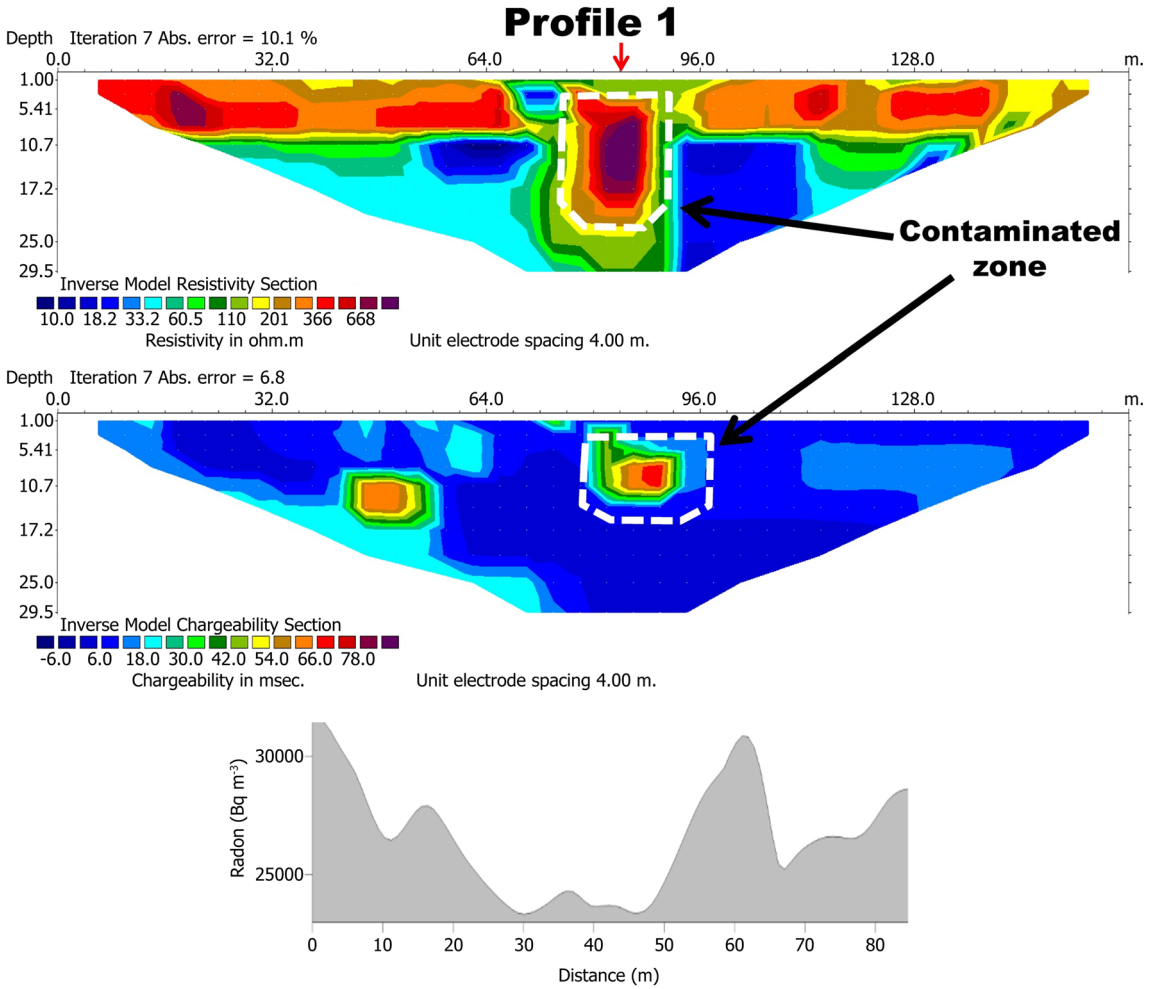

Fig. 5 Resistivity (DC) and induced polarization (IP) sections along profile 1 (for locations refer to Fig. 3a) at site 2a. Soil radon concentration at 80 cm depth along the profile is also reported for comparison. The red arrow on top of DC profile represents the intercept between the two profiles

5 and 6, respectively) in correspondence with high resistivity values. These regions have been accordingly delimited by white dotted lines. Their extension in depth is lower (up to 10–15 m) than corresponding areas in DC profiles (Figs. 5 and 6). Taking a closer look, the shape of soil volume with higher chargeability in profile 2 consists of two lobes opening around the high resistivity area, interpreted as an underground storage tank; the two lobes are connected by medium IP values (20 ms). Deepest portion of both IP sections are characterized by lower values, except for the left side of profile 1.

Summing up, high resistivity areas seem to be correlated with underground storage tank and contaminated plume. There is a good correspondence between high resistivity and high chargeability. This strengthens recent findings that both parameters are sensitive to hydrocarbons. According to the available literature (Johansson et al. 2015), it can be inferred that contamination in site 2a and b is due to the presence of LNAPL and not to DNAPL. Additionally, LNAPL is distributed as isolated droplets in the pores or trapped in the pore throats. However, to further support this model of NAPL distribution within the pore space, suitable laboratory simulation is required.

Discussion

Maps of radon activity concentration obtained for sites 1 (Fig. 2), 2a (Fig. 3a), and 2b (Fig. 3b) show areas with relatively low concentrations, interpreted as proxies for the presence of NAPLs in the subsoil (vadose zone). Average radon-deficit is actually about ten, two, and six times the value of radon concentration in the background for sites 1, 2a, and 2b, respectively. Larger differences not only are due to the amount of contaminant in the subsoil, but also depend on the higher soil water content (and/or lower soil permeability) which prevents soil gas release, emphasizing the effect of preferential solubility of radon into NAPLs. Higher deficit in site 1 is probably also dependent on the lower average temperature (13 °C)

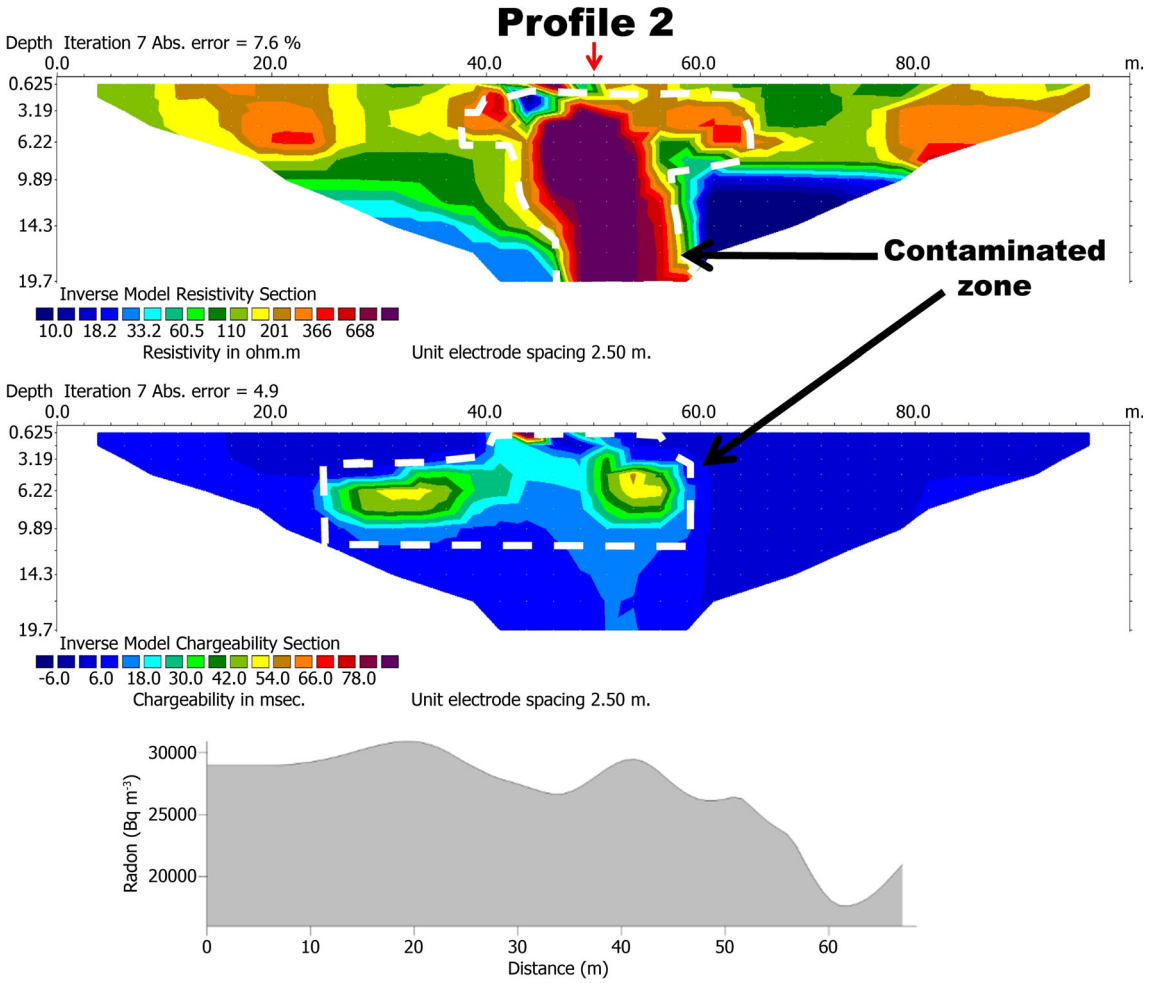

Fig. 6 Resistivity (DC) and induced polarization (IP) sections along profile 2 (for locations refer to Fig. 3) at site 2a. Soil radon concentration at 40 cm depth along the profile is also reported for comparison. The red arrow on top of DC profile represents the intercept between the two profiles

occurring in Roma during the end of February 2016, compared with correspondent March 2016 value in Kharagpur (25–27 °C). Moreover, radon deficit in site 2a is lower than in site 2b because sand/silt dominated alluvial sediments outcropping in the former area are more permeable than lateritic soil in the latter zone and are characterized by lower water contents (6 against 24%). Accordingly, estimations of residual NAPL for site 2a (1.5 kg per cubic meter of terrain) are one order of magnitude lower than for site 2b (11.8 kg per cubic meter of terrain) because of higher degassing, probably due to higher pore space interconnection (higher effective porosity), despite of quite similar total porosities. Moreover, soil radon changes across a single area are not due to evident variations of soil permeability which is generally constant in the three sites.

Radon deficit in the vadose zone of site 1 is attributed to the residual fraction of kerosene in the soil pores and is not influenced by NAPL vapors which are strongly reduced after more than 10 years from the spill. Even though the spillage is not recent, microbial degradation did not completely remove the kerosene, as the lack of a clear correlation between radon-deficit and high chargeability seems to suggest. This information could actually indicate that NAPL films of residual kerosene probably cover soil grains, inhibiting transfer of electrical charges through the soil (Shefer et al. 2013; Johansson et al. 2015). A rough correlation between high resistivity and radon deficit is observed and could be compatible with the reduced electrical conductivity of non-polar substances such as NAPLs in the subsoil.

Radon deficit at site 2a is probably due to residual gasoline in the vadose zone which extended up to 8 m below the ground in March 2016. Due to heavy precipitation during the rainy season, the annual water table fluctuations are within the range of 4–5 m (Garg et al. 2005; Central Groundwater Board—Government of India 2014). This implied that a smearing zone was created from the bottom of the petrol tank, located at 3 m depth, down to 8 m. This allowed a gradual and cyclic lateral migration of the gasoline over time. In any case, no direct information on the presence of a continuous free-phase plume floating over the water table is available. Soil

radon concentration along profiles 1 (Fig. 5) and 2 (Fig. 6) mostly decrease where higher electrical resistivity and chargeability extend deep, suggesting that these areas are probably contaminated with gasoline. The interpretation of these sections could be explained by the occurrence of gasoline as isolated droplets in the pores or trapped in the pore throats, as suggested by Johansson et al. (2015). This distribution could be consistent with a recent spill or a slow, but continuous leakage from the petrol tank. However, further studies such as laboratory simulations are needed to support this interpretation.

Finally, resistivity values in the background depend on the nature of terrains and mark very well the groundwater table, but a comparison between highest and lowest resistivity (or highest values in the contaminated site with respect to a close unpolluted reference area) can be used to qualitatively estimate the age of the spillage. According to the model proposed by Che-Alota et al. (2009) which associates the age of the spill with a progressive decrease of electrical resistivity due to partial microbial degradation of the contaminant mass and to volatilization, the highest values of electrical resistivity obtained for sites 1 (about 300 Ωm) and 2a (800–100 Ωm) confirms that the spill in Italy is older, whereas it is recent or in slow progress in India.

Conclusions

A multi-method approach based on soil radon deficit, resistivity, and induced polarization measurements to monitor NAPL contamination was applied in two study areas in Italy and India, characterized by different geological and climatological conditions. Some general conclusions exportable to other situations came out.

Radon deficit, intended as the ratio between soil radon in the polluted area and correspondent value in a background reference site, identifies the contaminated area. It is influenced by the seasonal soil condition (water content, permeability, temperature) and can be used to quantify the spill. Better results are obtained in winter or at middle latitude locations (such as central Italy) compared with low-latitude sites (such as West Bengal, India) with tropical climate, because both soil radon and volatile organic compounds (such as NAPLs) are more easily released at high temperature, reducing the sensitivity of the radon-deficit technique.

Residual gasoline in sites 2a and 2b were respectively estimated at 1.5 and 11.8 kg per cubic meter of terrain. Site 2a with higher effective porosity and lower water content lost more gasoline compared with site 2b characterized by higher water content and lower gas permeability.

Finally, a direct correlation between radon deficit at shallow depth and highest electrical resistivity at greater depth could be used as proxy for the presence of the contaminant in the aquifer. A progressive reduction of radon deficit over time (corrected for seasonal-induced variations), coupled to a reduction of electrical resistivity and a change of correlation with chargeability, could be used to evaluate the progress of remedial actions such as soil venting or dual-phase extraction. Further research is needed to explore this.

Acknowledgements This research was carried out in the frame of TECO projects (Technological eco-innovations for the quality control and the decontamination of polluted waters and soils) funded by the European Union. A grant was attributed to Mauro Castelluccio to visit Indian Institute of Technology at Kharagpur for 40 days and exchange knowledge and experience on NAPLs contamination. Derek Lane-Smith (Durridge Co.) is warmly acknowledged because he made available a RAD7 instrument in Kharagpur (India), during the stay of Mauro Castelluccio there. Durridge people in India facilitated the expedition of the radon monitor from Delhi to Kharagpur.

Appendix.

Starting from Eq. (1), proposed by Schubert (2015) to calculate soil radon concentration in the pore space (C_∞), we have developed a new calculation, Eq. (2), where radon concentration in the polluted sites is firstly compared to soil radon values in close unpolluted areas to calculate the radon deficit (Di). Equilibrium radon concentration in the background is determined using a simplified version of Eq. (1):

$$C_\infty = \varepsilon A_{\mathrm{Ra}} \rho_d / n \tag{3}$$

From the comparison of Eqs. (1) and (3), it turns out that

$$D_i = 1/\left(1-S_{\mathrm{F}} + K_{\mathrm{W/SG}} S_{\mathrm{F}} \left(1-X_{\mathrm{NAPL}}\right) + K_{\mathrm{NAPL/SG}} X_{\mathrm{NAPL}} S_F\right) \tag{4}$$

Now, the total fluid saturation of the pore space (S_{F}) is the sum of S_{NAPL} and S_{W}, which are the pores fractions occupied by NAPL (S_{NAPL}) and water (S_{W}), respectively, and these two terms can be expressed as follows:

$$S_{\mathrm{NAPLi}} = \mathrm{NAPL_{Pi}}/\left(\left(\gamma_{\mathrm{NAPL}}/\gamma_{\mathrm{di}}\right)-\left(\gamma_{\mathrm{NAPL}}/\gamma_{\mathrm{s}}\right)\right) \tag{5}$$

$$S_{\mathrm{W\,i}} = W_{\mathrm{Pi}}/\left(\left(\gamma_{\mathrm{Wi}}/\gamma_{\mathrm{di}}\right)-\left(\gamma_{\mathrm{Wi}}/\gamma_{\mathrm{s}}\right)\right) \tag{6}$$

or simplifying, $S_{\mathrm{NAPL\ i}} = \mathrm{NAPL_{Pi}}/A$ and $S_{\mathrm{W\ i}} = W_{\mathrm{Pi}}/B$

where

$$A = \left(\left(\gamma_{\mathrm{NAPL}}/\gamma_{\mathrm{di}}\right)-\left(\gamma_{\mathrm{NAPL}}/\gamma_{\mathrm{s}}\right)\right) \tag{7}$$

$$B = \left(\left(\gamma_{\mathrm{Wi}}/\gamma_{\mathrm{di}}\right)-\left(\gamma_{\mathrm{Wi}}/\gamma_{\mathrm{s}}\right)\right) \tag{8}$$

then,

$$S_{\mathrm{F}\ i} = \left(\mathrm{NAPL_{Pi}}/A\right) + \left(\mathrm{W_{Pi}}/B\right) \tag{9}$$

If parameters defined in equations from (5) to (9) are inserted in Eq. (4) and then the latter is developed and solved

with respect to $NAPL_{Pi}$, we obtain Eq. (2), where the following polynomials are defined:

$$C = (W_{Pi}/B) - (D_i W_{Pi}/B) + \left(D_i {W_{Pi}}^2/B^2\right) - \left(D_i K_1 {W_{Pi}}^2/B^2\right) \quad (10)$$

$$D = [D_i W_{Pi}/AB)] - 2\left[D_i K_1 W_{Pi}/(AB)\right] + (1/A) - (D_i/A) \quad (11)$$

$$E = \left(D_i/A^2\right) - \left(D_i K_1/A^2\right) \quad (12)$$

$$F = [D_i K_2 W_{Pi}/(AB)] - [D_i K_1 W_{Pi}/(AB)] \quad (13)$$

$$G = \left(D_i K_2/A^2\right) - \left(D_i K_1/A^2\right) \quad (14)$$

$$H = E - G \quad (15)$$

$$J = D - F \quad (16)$$

Note that $K_{W/SG}$ and $K_{NAPL/SG}$ are labeled as K_1 and K_2, respectively.

The solution to the following calculation:

$$H\ {NAPL_{Pi}}^2 + J\ NAPL_{Pi} + C = 0 \quad (17)$$

is the above mentioned Eq. (2):

$$NAPL_{Pi} = \frac{-J \pm \sqrt{J^2 - 4CH}}{2H}$$

where actually two solutions, one positive and one negative, are provided, but only the positive one (deriving from the negative sign in front of the square root) is meaningful. Calculated fractions of NAPL in the pore space ($NAPL_{Pi}$) of sites 2a and 2b are reported in Table S1 and S2 for all the stations of the grids. Table 1 lists other parameters used for calculation.

References

Candansayar ME (2008) Two-dimensional individual and joint inversion of three and four-electrode array dc resistivity data. J Geophys Eng 5(3):290–300. https://doi.org/10.1088/1742-2132/5/3/005

Carapezza ML, Barberi F, Tarchini L, Ranaldi M, Ricci T, Barrancos J, Fischer C, Lucchetti C, Melian G, Perez N, Tuccimei P, Vogel A, Weber K (2012) Hazardous gas emissions from the flanks of the quiescent Colli Albani volcano (Rome, Italy). Appl Geochem 27(9):1767–1782. https://doi.org/10.1016/j.apgeochem.2012.02.012

Castelluccio M, De Simone G, Lucchetti C, Moroni M, Salvati F, Tuccimei P (2015) A new technique to measure in situ soil gas permeability. J Geochem Explor 148:56–59. https://doi.org/10.1016/j.gexplo.2014.08.002

Central Groundwater Board, Ministry of Water Resources—Government of India (2014) Ground water year book of West Bengal & Andaman & Nicobar Islands (2013–2014). Technical report. Series D

Chatterjee S, Paul AK, Roy U (2003-2004) Some observations on the diverse lateritic landscape of Subarnarekha—Kangsabati—Silabati interfluves of Paschim Medinipur, West Bengal. Indian J Geogr Environ 8-9:82–95

Che-Alota V, Atekwana EA, Atekwana EA, Sauck WA, Werkema DD (2009) Temporal geophysical signatures from contaminant-mass remediation. Geophysics 74(4):B113–B123. https://doi.org/10.1190/1.3139769

Chiodini G, Valenza M. (2007) Results of INGV-DPC-V5 project: the catalogue of Italian gas emissions. googas.ov.ingv.it. Accessed 13 Mar 2015

Dahlin T, Zhou B (2004) A numerical comparison of 2-D resistivity imaging with10 electrode arrays. Geophys Prospect 52(5):379–398. https://doi.org/10.1111/j.1365-2478.2004.00423.x

De Simone G, Galli G, Lucchetti C (2015) Using natural radon as a tracer of gasoline contamination. Procedia Earth Planet Sci 13:104–107. https://doi.org/10.1016/j.proeps.2015.07.025

De Simone G, Lucchetti C, Galli G, Tuccimei P (2016) Correcting for H_2O interference using electrostatic collection-based silicon detectors. J Environ Radioact 162-163:146–153. https://doi.org/10.1016/j.jenvrad.2016.05.021

De Simone G, Lucchetti C, Pompilj F, Galli G, Tuccimei P, Curatolo P, Giorgi R (2017) Soil radon survey to assess NAPL contamination from an ancient spill. Do kerosene vapors affect radon partition ? J Environ Radioact 171:138–147. https://doi.org/10.1016/j.jenvrad.2017.02.014

Garg KK, Jha MK, Kar S (2005) Field investigation of water movement and nitrate transport under perched water table conditions. Biosyst Eng 92(1):69–84. https://doi.org/10.1016/j.biosystemseng.2005.05.016

Giordano G, Carapezza ML, Della Monica G, Todesco M, Tuccimei P, Carlucci G, De Benedetti AA, Gattuso A, Lucchetti C, Piersanti M, Ranaldi M, Tarchini L, Pagliuca NM, Ricci T, Facchini S, D'Ambrosio F, Misuraca M, Bonamico A, Geshi N (2016) Conditions for long-lasting gas eruptions: the 2013 event at Fiumicino International airport (Rome, Italy). J Volcanol Geotherm Res 325:119–134. https://doi.org/10.1016/j.jvolgeores.2016.06.020

Johansson S, Fiandaca G, Dahlin T (2015) Influence of non-aqueous phase liquid configuration on induced polarization parameters: conceptual models applied to a time-domain field case study. J Appl Geophys 123:295–309. https://doi.org/10.1016/j.jappgeo.2015.08.010

Loke MH (1997) RES2DINV ver. 3.3 for Windows 3.1, 95, and NT Advanced Geosciences, Inc. 66

Loke MH, Barker RD (1996) Rapid least-squares inversion of apparent resistivity pseudo sections by a quasi-Newton method. Geophys Prospect 4:131–152

Machiwal D, Jha MK (2016) Exploring hydrogeology and groundwater dynamics in a lateritic terrain of West Bengal, India, under limited data conditions. Environ Earth Sci 75:article 831

Mackay DM, Cherry JA (1989) Groundwater contamination: pump-and-treat remediation. Environ Sci Technol 23(6):630–636. https://doi.org/10.1021/es00064a001

Rogie JD, Kerrick DM, Chiodini G, Frondini F (2000) Flux measurements of nonvolcanic CO_2 emission from some vents in central Italy. J Geophys Res 105(B4):8435–8445. https://doi.org/10.1029/1999JB900430

Sauck WA, Atekwana EA, Nash MS (1998) High conductivities associated with an LNAPL plume imaged by integrated geophysical techniques. J Environ Eng Geophys 2:203–212

Scanlon BR, Mukherjee A, Gates J, Reedy RC, Sinha AK (2010) Groundwater recharge in natural dune systems and agricultural ecosystems in the Thar Desert region, Rajasthan, India. Hydrogeol J 18(4):959–972. https://doi.org/10.1007/s10040-009-0555-7

Schubert M (2015) Using radon as environmental tracer for the assessment of subsurface non-aqueous phase liquid (NAPL) contamination—a review. Eur Phys J Special Topics 224(4):717–730. https://doi.org/10.1140/epjst/e2015-02402-3

Schubert M, Lehmann K, Paschke A (2007) Determination of radon partition coefficients between water and organic liquids and their utilization for the assessment of subsurface NAPL contamination. Sci Total Environ 376(1-3):306–316

Semprini L, Hopkins OS, Tasker BR (2000) Laboratory, field, and modeling studies of Radon-222 as a natural tracer for monitoring NAPL contamination. Transp Porous Med 38(1/2):223–240. https://doi.org/10.1023/A:1006671519143

Shefer I, Schwartz N, Furman A (2013) The effect of free-phase NAPL on the spectral induced polarization signature of variably saturated soil. Water Resour Res 49(10):6229–6237. https://doi.org/10.1002/wrcr.20502

Slater LD, Lesmes D (2002) IP interpretation in environmental investigations. Geophysics 67(1):77–88. https://doi.org/10.1190/1.1451353

Tuccimei P, De Simone G, Curatolo P, Giorgi R, Lucchetti C, Castelluccio M, Calì A (2014) Tracing NAPLs contamination in the vadose zone using soil radon. Rend online Soc Geol It 33:100–103

Weigel F (1978) Radon. Chem Ztg 102:287–299

Zhang Q, Davis LC, Erickson LE (1998) Effect of vegetation on transport of groundwater and nonaqueous phase liquid contaminants. J Hazard Subst Res 1:8–20